Macro-Scale Basis Functions for the Method of Moment Analysis of Large Periodic Microstrip Arrays

(*Invited paper*)

A. Cucini and S. Maci
Dipartimento di Ingegneria dell'Informazione, University of Siena, Via Roma 56, 53100 Siena, Italy
E-mail: cucini@dii.unisi.it, macis@dii.unisi.it

Abstract – This paper presents a hybrid numerical-asymptotic technique for the analysis of large periodic microstrip arrays. In the solution of a typical array problem, both macro-scale and element-scale spatial variations of the electromagnetic quantities are encountered. For large periodic arrays, the truncated periodicity induces a macro-scale behavior that is weakly dependent on the radiating elements themselves, but strongly dependent on the array periodicity and phasing. To incorporate this global phenomena, appropriate macro-scale functions are used in the framework of a method of moment solution. These macro-functions are associated to Floquet wave induced diffracted waves and guided waves, excited at the array boundary. The properties of these functions are discussed here. The technique is applied to the simple but significant case of printed dipole array, in order to demonstrate the effectiveness of the approach.

I. INTRODUCTION

Modelling large periodic array antennas involves critical issues relevant to the intrinsic multi-scale features of these structures. Macro-scale spatial variations coexist with element-scale variations which require much-smaller than wavelength discretization. These latter are due to element shape, and are responsible of quasi-static interactions which often dominate the frequency response of the antenna input impedance. On the other side, macro-scale variations are strongly dependent on the periodicity of the array and on the phasing of the excitation. Aim of this paper is to highlight such basic macro-scale phenomena and to incorporate them, as array-domain basis functions, into a full-wave method of moment (MoM) analysis of the entire structure. In order to simplify the treatment, we will refer to simple configurations constituted by finite periodic arrays of printed dipoles on a grounded dielectric slab.

The approach based on the MoM solution of integral equations is largely used for array problems. It is well known, however, that conventional formulations are severely limited by the problem size. Large and very-large arrays are often treated using the approximation of infinite periodic structure [1], [2]. Under this hypothesis, the electromagnetic analysis is reduced to that of a single periodic cell, by representing the Green's function of the infinite array as a summation of Floquet waves (FWs). This approach, although computationally very efficient, cannot be rigorously applied when the array has a finite extension, since FWs do not constitute a complete basis. The truncation effects are particularly relevant for elements near the array edge and, for wide scan angles, even for elements at the center of the array. Moreover, in the case of arrays printed on a stratified dielectric media or with a dielectric cover, the array truncation may excite guided waves (either surface waves (SWs) or leaky waves (LWs)) that cannot be predicted through the analysis of the infinite periodic array. These guided waves cause large oscillations of the current amplitude over the array and are responsible of scan-blindness effects in phased array antennas [3]. The presence of SWs can be detected also in finite free-space dipole arrays, when the array operates below the resonance and the inter-element spacing is smaller than half of a wavelength [4].

On the other side, a brute force application of the MoM to the finite array leads indeed to large, dense and sometimes ill-conditioned matrices, with a consequent huge memory occupation and CPU

1054-4887 ' 2006 ACES

time. In order to overcome these problems, synthetic [5] or characteristic [6] basis functions have been recently proposed. These basis functions are defined from the solution of small-size numerically-tractable problems, and then used in the MoM solution of the large problem. This allows one to incorporate the small- and intermediate-scale features of the structure, while maintaining a reduced number of unknowns.

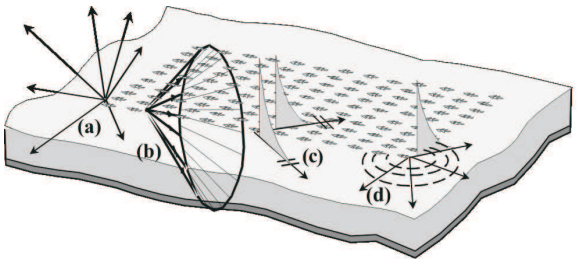

Fig. 1. Waves excited by Floquet waves at a finite array of linearly phased elementary dipoles printed on a grounded dielectric slab: (a) spherical vertex-excited (space) diffracted wave, (b) conical edge-excited (space) diffracted wave, (c) planar edge-excited surface wave, (d) cylindrical vertex-excited surface wave.

In this paper, the use of problem-matched macro-scale basis functions is proposed, to obtain a compression of the MoM matrix, provided that a suitable integral equation is derived in order to isolate the edge-induced phenomenology. The basic principles of this technique have been introduced in [8]-[10] for free-space arrays, such as dipole or slot arrays as well as open-ended waveguide arrays, and it is extended here to arrays composed of planar radiating elements printed on or embedded in dielectric stratifications.

The definition of macro-scale functions is based on a high-frequency analysis of the radiation and scattering by truncated periodic arrays. The frequency-domain phenomenology of wave excitation in truncated periodic arrays has been extensively analyzed in a series of recent papers dealing with semi-infinite and sectoral arrays in free space [11]-[13] and in stratified media [14]. The various species of diffracted and guided waves excited in a truncated periodic array are illustrated in Fig. 1, referring to a finite array of elementary electric dipoles on a infinite grounded dielectric slab. Each periodicity-induced FW excites conical and spherical space diffracted waves emanating from array edges and corners, respectively. These wave contributions are also present when the array is in free-space. In addition, plane and cylindrical guided waves (which can be either SWs or LWs) are excited at edges and corners of the array. The direction of propagation of edge-induced diffracted and guided waves is such as to match the phase velocity of the dominant FW along the edge. As we will see next, while for elementary dipoles the SW/LW wavenumber is dictated by the multilayered dielectric environment [14], for actual finite-size patches the SW/LW wavenumber is influenced also by the presence of the periodic metallization, and its calculation cannot leave apart the solution of the dispersion equation.

The paper is organized as follows. Sec. III summarizes the formulation that allows to separate the different features of the array: the original integral equation (IE) is decomposed into two equations, one relevant to the infinite periodic problem, and one relevant to the truncation-induced current. The infinite periodic array IE is solved in Sec. IV by using a conventional spectral-domain FW approach. Then Sec. V presents the solution of the integral equation associated to the truncation effects. Particular emphasis is given to the identification and construction of the array-domain basis function, which allows for a numerically efficient and physically appealing solution. Numerical results are presented in Sec. VI to show the accuracy of the method as compared with a conventional element-by-element technique. Finally, some concluding remarks are traced in Sec. VII.

II. INTEGRAL EQUATIONS FORMULATION

The geometry of a finite rectangular periodic array of printed dipoles is shown in Fig. 2. The array is composed by x-oriented dipoles, with length L and width W ($W \ll L$), arranged on a rectangular grid, with spatial periodicity denoted by d_x and d_y. The grounded dielectric slab has thickness h and relative permittivity ε_r. The array excitation may be provided by an incident plane wave (Fig. 2a) or by delta-gap sources (Fig. 2b), with uniform amplitude and linear phase $e^{-j\mathbf{k}_0\cdot\mathbf{r}}$, where an $e^{j\omega t}$ time dependence has been assumed and

suppressed. In the previous expression, $\mathbf{r} = x\hat{x} + y\hat{y}$ is the position vector in an arbitrary point of the array plane, $\mathbf{k}_0 = \gamma_x\hat{x} + \gamma_y\hat{y}$ is the transverse-to-z wavevector component of the excitation field, where $\gamma_x = k\sin\theta_0\cos\phi_0$, $\gamma_y = k\sin\theta_0\sin\phi_0$, $k = \omega\sqrt{\epsilon_o\mu_o}$ is the free-space wavenumber, and (θ_0, φ_0) denote the direction of the scattered/radiated main beam in the conventional spherical coordinate system.

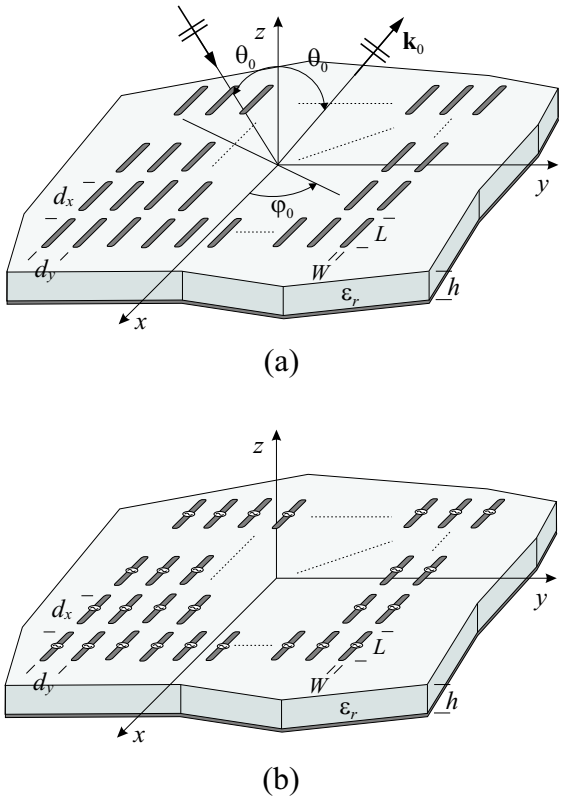

Fig. 2. Finite rectangular planar periodic array of metallic dipoles printed on a grounded dielectric slab. (a) Scattering problem: incident plane-wave excitation; (b) Radiation problem: delta-gap excitation.

An electric current distribution $\mathbf{J}$ is defined on the surface of the printed dipoles. Imposing the vanishing of the total electric field at the perfectly conducting dipoles yields the electric field integral equation (EFIE)

$$\chi_A \mathbf{E}^s_{tan}(\mathbf{J}) = -\chi_A \mathbf{E}^{imp}_{tan} \tag{1}$$

where $\mathbf{E}^s_{tan}(\mathbf{J})$ is the tangential (to the xy-plane) component of the electric field scattered by the unknown current distribution $\mathbf{J}$ and $\mathbf{E}^{imp}_{tan}$ is the impressed tangential electric field. In Eq. (1), A denotes the portion of the xy-plane occupied by the conducting dipoles and χ_A is the characteristic function of A ($\chi_A(\mathbf{r}) = 1$ if $\mathbf{r} \in A$, $\chi_A(\mathbf{r}) = 0$ if $\mathbf{r} \notin A$).

Following the procedure introduced in [7], [8], the unknown electric current is decomposed as

$$\mathbf{J} = \chi_A \mathbf{J}_\infty + \mathbf{J}_f \tag{2}$$

where $\mathbf{J}_\infty$ is the infinite periodic array current, and $\mathbf{J}_f$ denotes the 'fringe' current, i.e. the perturbation current induced by the truncation. We define $\chi_A\mathbf{J}_\infty$ as the Physical Optics (PO) approximation current, where the PO terminology is used with reference to the abrupt truncation (via the function χ_A) of the infinite array current on A. The current $\mathbf{J}_\infty$ is the solution of the EFIE pertinent to the infinite periodic array,

$$\chi_\infty \mathbf{E}^s_{tan}(\mathbf{J}_\infty) = -\chi_\infty \mathbf{E}^{imp}_{tan} \tag{3}$$

where χ_∞ is the characteristic function of the dipole region of the infinite periodic array. Note that the infinite array characteristic function can be written as $\chi_\infty = \chi_A + \chi_{A^*}$, where A^* is the portion of the xy-plane external to the array region A.

By inserting (2) into (1), and successively subtracting (3) from (1), yields the Fringe Integral Equation (FIE)

$$\chi_A \mathbf{E}^s_{tan}(\mathbf{J}_f) = \chi_A \mathbf{E}^s_{tan}(\chi_{A^*}\mathbf{J}_\infty) \tag{4}$$

whose unknown function is the fringe current $\mathbf{J}_f$. The forcing term of Eq.(4), $\chi_A \mathbf{E}^s_{tan}(\chi_{A^*}\mathbf{J}_\infty)$, represents the tangential component of the electric field radiated by the infinite array current truncated on the complementary array region A^*. (Note that this term is known once the infinite array current has been computed.) Thus, the FIE (4) interprets the fringe current $\mathbf{J}_f$ as the perturbation, with respect to the PO approximation, which is necessary to compensate for the absence of radiation from the suppressed current $\chi_{A^*}\mathbf{J}_\infty$, in order to ensure the boundary conditions (1) on A. The total current of the finite array is found, through relationship (2), by the MoM solution of Eq. (3) and (4), with the process described next.

III. INFINITE PERIODIC ARRAY SOLUTION

The first step of the procedure is the MoM solution of the integral equation (3) relevant to the

infinite periodic array. The problem is solved by using a conventional periodic MoM [1]. The current $\mathbf{J}_\infty$ of the infinite periodic array respects the pseudo-periodic property imposed by the Floquet condition

$$\mathbf{J}_\infty(\mathbf{r}) = \mathbf{J}_0(\mathbf{r})e^{-j\mathbf{k}_0\cdot\mathbf{r}} \tag{5}$$

where $\mathbf{J}_0(\mathbf{r})$ is a doubly periodic function with periodicity (d_x, d_y). Thus, the MoM computation of the infinite array current is reduced to that of a single periodic cell, by representing the Green's function kernel as a summation of FWs. The electric current $\mathbf{J}_0$ on the dipole of the reference cell is expanded into a set of basis functions (either entire or sub-domain functions). By applying the Galerkin method, the integral equation (3) is reduced to the algebraic linear system

$$\overline{\overline{Z}}_\infty(\mathbf{k}_0, \omega)\bar{I} = \bar{V}(\mathbf{k}_0, \omega) \tag{6}$$

where, for the sake of convenience, we have explicitated the dependence of the matrix $\overline{\overline{Z}}_\infty$ and of the vector $\bar{V}$ (and consequently of the unknown coefficients vector $\bar{I}$) on the excitation wavevector $\mathbf{k}_0$ and (angular) frequency ω.

IV. FRINGE INTEGRAL EQUATION SOLUTION

The solution of the FIE is expressed in terms of diffracted and guided wave contributions associated to the truncation effects. The unknown fringe current $\mathbf{J}_f$ is expanded using array-domain basis functions, associated to diffracted waves $\mathbf{F}^d_{i,\mu}$ and to guided waves $\mathbf{F}^{GW}_{i,\nu}$,

$$\mathbf{J}_f(\mathbf{r}) \approx \sum_i \left[\sum_\mu a_{i,\mu}\mathbf{F}^d_{i,\mu}(\mathbf{r}) + \sum_\nu b_{i,\nu}\mathbf{F}^{GW}_{i,\nu}(\mathbf{r}) \right] \tag{7}$$

where $a_{i,\mu}$ and $b_{i,\nu}$ are unknown coefficients to be determined through a MoM scheme. In the previous expressions, the first subscript ($i = 1, \ldots, 4$) denotes the edge numbering of the rectangular array, while the second subscript μ (ν) denotes the diffracted (guided) wave. The array-domain basis functions are obtained by multiplication of the element-scale current $\mathbf{J}^d_{i,\mu}$ and $\mathbf{J}^{GW}_{i,\nu}$ with the macro-scale functions $f^d_{i,\mu}$ and $f^{GW}_{i,\nu}$, respectively,

$$\mathbf{F}^d_{i,\mu}(\mathbf{r}) = \sum_{\mathbf{r}_{nm}\in A} \mathbf{J}^d_{i,\mu}(\mathbf{r} - \mathbf{r}_{nm}) f^d_{i,\mu}(\mathbf{r}_{nm}) \tag{8}$$

$$\mathbf{F}^{GW}_{i,\nu}(\mathbf{r}) = \sum_{\mathbf{r}_{nm}\in A} \mathbf{J}^{GW}_{i,\nu}(\mathbf{r} - \mathbf{r}_{nm}) f^{GW}_{i,\nu}(\mathbf{r}_{nm}). \tag{9}$$

Details on the selection and construction of the macro-scale and element-scale functions are given in the following paragraph. It is worth noting that the number of basis functions is completely independent of the number of array elements, thus allowing the numerical analysis of arbitrarily large arrays with the same number of unknowns.

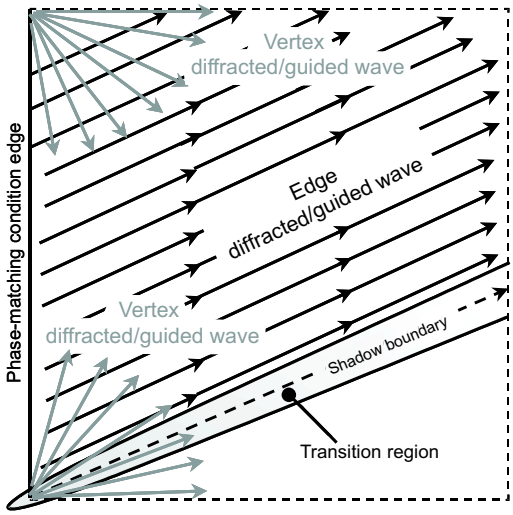

Fig. 3. Ray description of macro-scale diffracted and guided wave basis functions. The macro-scale function includes an edge contribution plus two end-point vertex contributions, ensuring the unform continuity of the current at the shadow boundaries. The propagation constant along the edge is fixed by the excitation according the generalized Fermat condition in (13) and (14).

A. Macro-scale functions: FW-matched diffracted and guided waves

Each macro-scale function $f^d_{i,\mu}$, $f^{GW}_{i,\nu}$ includes an edge contribution plus two end-point vertex contributions, which ensure the uniform continuity to the current (Fig. 3). The edge diffracted waves are cylindrical wave which asymptotically propagate with the speed of light and decay like $\rho_i^{-3/2}$, where ρ_i denotes the distance of the observation point from the i-th edge. The vertex diffracted waves are spherical waves with ray spreading r_i^{-2}, being r_i the distance from the i-th vertex. The exact expression of the FW-induced space diffracted waves

and the relevant phenomenology is given in [8]-[10]. The edge-excited guided waves decay as ρ_i^0 (inhomogeneous plane waves), thus providing the dominant contribution to the fringe current $\mathbf{J}_f$. The propagation constant of the guided waves is dictated by the environment and by the shape and periodicity of the microstrip array elements. The problem of the identification of the guided waves wavenumbers is addressed in the following sub-section. The vertex-excited terms are cylindrical waves originating from the end-point of the edge with ray spreading $r_i^{1/2}$. In this latter case, we approximate the wavenumber with that of the relevant edge term, by using the criterion to compensate for the discontinuities at the shadow boundaries. Actually, the propagation constant of the guided waves excited in the array varies with the azimuthal angle since the 'effective' periodicity of the medium depends on this angle. Nevertheless, it will be shown from the numerical results that this approximation does not affect the accuracy of the method.

B. Identification of FW-matched guided wavenumber

The propagation constant of the guided waves excited in the microstrip array differs from that of the grounded slab modes, since it is affected by the periodic loading effect of the finite-size metallic patches. Indeed, the guided waves excited in the microstrip array can be seen as a periodicity-induced perturbation of those supported by the bare grounded slab structure. The individuation of the propagation constant of the array guided waves is achieved through the solution of a homogeneous resonance equation [15] which is obtained from Eq. (6) by removing the excitation term, namely

$$\overline{\overline{Z}}_\infty(\mathbf{k}^{GW},\omega)\bar{I}=0. \tag{10}$$

For any frequency, this equation admits non-trivial solutions when the matrix determinant vanishes, i.e.,

$$\det[\overline{\overline{Z}}_\infty(\mathbf{k}^{GW},\omega)]=0 \tag{11}$$

where the unknown is the guided-wave complex transverse wavevector

$$\mathbf{k}^{GW}=k_x^{GW}\hat{x}+k_y^{GW}\hat{y} \qquad GW=SW,LW. \tag{12}$$

When the propagation wavenumber is real ($k_{x,y}^{SW}=\beta_{x,y}^{SW}$), the corresponding mode is a bound (non-radiating) SW. When the propagation constant is complex ($k_{x,y}^{LW}=\beta_{x,y}^{LW}-j\alpha_{x,y}^{LW}$), the mode is a (radiating) LW. The elements of the matrix $\overline{\overline{Z}}_\infty$ involve a double summation in the spectral domain over the transverse FW wavenumbers $k_{xp}^{GW}=k_x^{GW}+2\pi p/d_x$ and $k_{yq}^{GW}=k_y^{GW}+2\pi q/d_y$. Different branch choices are possible for the doubly infinite number of spatial harmonics. The branch choice for the wavenumber in the dielectric region $k_{zd,pq}=\sqrt{\varepsilon_r k^2-k_{xp}^2-k_{yq}^2}$ (the superscript GW has been suppressed for simplicity) is arbitrary, since the Green's function is an even function of $k_{zd,pq}$. Each wavenumber in the semi-infinite air region $k_{z,pq}=\sqrt{k^2-k_{xp}^2-k_{yq}^2}$ may be chosen to be proper (negative imaginary part, corresponding to a spatial harmonic that exponentially decays in the z-direction) or improper (positive imaginary part, corresponding to a harmonic exponentially increasing in the z-direction). Since only physical solutions must be retained, the branches are chosen according the rules given next. Before proceeding further, it is worth emphasizing that, since we are looking for edge-excited guided waves, one component of the propagation constant (the one along the edge) is imposed by the phasing of the excitation.

In the SW case, the FW phase-matching condition [14] along the edges of the array imposes

$$\beta_x^{SW}=k_{xp}^{FW} \quad \text{or} \quad \beta_y^{SW}=k_{yq}^{FW} \tag{13}$$

for edges along x or y, respectively, where $k_{xp}^{FW}=\gamma_x+2\pi p/d_x$ and $k_{yq}^{FW}=\gamma_y+2\pi q/d_y$ are the FW transverse wavenumbers. Consequently, the only unknown is the real propagation constant orthogonal to the edge. In this case, all FW harmonics are in the slow-wave region and the proper branch choice is taken.

In the LW case, the phase-matching condition imposes

$$\begin{aligned}\beta_x^{LW}&=k_{xp}^{FW},\ \alpha_x^{LW}=0\\ \beta_y^{SW}&=k_{yq}^{FW},\ \alpha_y^{LW}=0\end{aligned} \tag{14}$$

for edges along x or y, respectively. Note that, since the transverse components of FW wavevectors are real, the LW attenuation constant along the edges is always zero. In this case, the unknowns are the propagation and attenuation constant orthogonal to the edge. For a radiating fast-wave harmonic the physical solution correspond to the proper branch choice when the harmonic is a backward wave (the

group velocity is in opposite direction with respect to the phase velocity), and to the improper one when the harmonic is a forward wave [16].

Finally we note that, since in practical phased array antenna or FSS problems only one FW harmonic is propagating, the couple of indices p, q in (13) and (14) reduces to $p, q = (0, 0)$.

C. Element-scale functions

The element current distribution $\mathbf{J}_{i,\mu/\nu}^{d/GW}(\mathbf{r})$, associated to both diffracted and guided waves, has to be determined, to construct the basis functions (8) and (9).

In the case of guided-wave current, $\mathbf{J}_{i,\nu}^{GW}(\mathbf{r})$ represents the eigenfunction of the homogeneous system (10), which can be computed by setting to unity one element of the vector $\bar{I}$ and then solving for the remaining elements [17].

In the case of diffracted-wave functions, the element current on the dipoles $\mathbf{J}_{i,\mu}^{d}(\mathbf{r})$ is assumed of resonant type, without care on the sub-wavelength details, which are indeed described by the infinite array solution. For more complicated element shapes, synthetic basis functions are generated by solving a periodic array problem with a suitable excitation [18].

V. NUMERICAL RESULTS

In this section, a sample of numerical results is shown to validate the above technique and to highlight some typical truncation effects of finite microstrip arrays. The results obtained with this technique (labelled $\mathrm{T(FW)^2}$) are compared with those from a conventional element-by-element MoM (El.-by-el. MoM) and with the (windowed) infinite array approximation (PO approx.). In all cases, the current on the dipoles is expanded in terms of PWS basis functions.

First, a 41×41 array is considered, with dipole length $L = 0.6$ cm, width $W = 0.1$ cm, and periodicity $d_x = d_y = 0.8$ cm. The dielectric substrate has relative permittivity $\varepsilon_r = 10.2$ and thickness $h = 0.1905$ cm. An incident TM-polarized plane wave is assumed to illuminate the array, with the scattered main beam angles $\theta_0 = 40^o$ and $\varphi_0 = 20^o$. The operating frequency is $f = 7$ GHz. The propagation constants of the guided waves excited at the edges of the array are computed by solving the resonance equation (11). Only one real solution is found, corresponding to a non-radiating SW. Complex roots associated to LWs are neglected due to the high values of the attenuation constant. The propagation constant of the SW excited by the y-oriented edges is given by Eq. (11), with the $k_y^{GW} = k \sin\theta_0 \sin\varphi_0 = 0.22k$, that yields $k_x^{GW} = \beta_x = 1.197k$. For the SW excited by the x-oriented edges, the solution of Eq. (11), with $k_x^{GW} = k \sin\theta_0 \cos\varphi_0 = 0.604k$, gives $k_y^{GW} = \beta_y = 0.920k$. Thus, the transverse propagation constant of the SW supported by the array is $k^{GW} = |\mathbf{k}^{GW}| = 1.217k$ for the mode excited by the y-

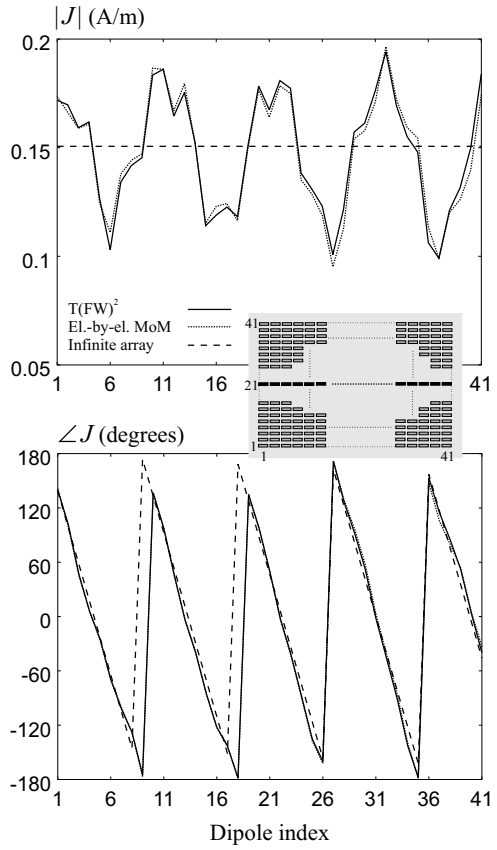

Fig. 4. Magnitude (in A/m) and phase (in degrees) of the surface electric current sampled at the centers of the dipoles on the central row of the array. Results refers to a 41×41 array of dipoles with $L = 0.6$ cm, $W = 0.1$ cm, $d_x = 0.8$ cm, and $d_y = 0.8$ cm. The dielectric substrate has $\varepsilon_r = 10.2$ and $h = 0.1905$ cm. The array is excited by an incident TM-polarized plane wave with $\theta_0 = 40^o$ and $\varphi_0 = 20^o$. The operating frequency is $f = 7$ GHz.

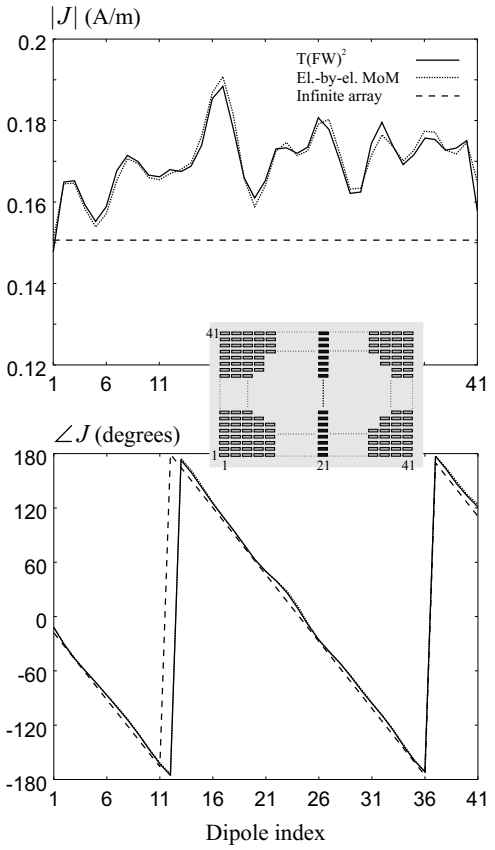

Fig. 5. Magnitude (in A/m) and phase (in degrees) of the surface electric current sampled at the centers of the dipoles on the central row of the array. Results refers to the 41×41 array of dipoles described in the caption of Fig. 4.

oriented edges, and $k^{GW} = |\mathbf{k}^{GW}| = 1.1k$ for the mode excited by the the x-oriented edges. Note that the phase constant of the SWs excited at two orthogonal edges differs each other, due to the anisotropy of the *effective* periodic medium. Figs. 4 and 5 present the electric current (amplitude and phase), sampled at the centers of each dipole, for the dipoles on the central row and on the central column of the array, respectively. An excellent agreement is found between the present technique (solid line) and the reference solution (dotted line). Also the infinite array data (dashed line) are shown in the diagrams, in order to appreciate the influence of the fringe current contributions. In the E-plane (Fig. 4), this influence can be quantified in terms of a large oscillation of the current amplitude around the value of the infinite array level. The normalized far

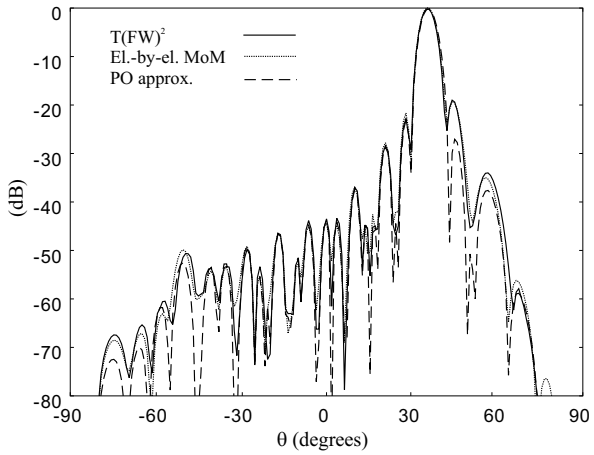

Fig. 6. Normalized far field scattered by the array on the incidence plane. Results refers to the 41×41 array of dipoles described in the caption of Fig. 4.

field scattered by the array on the incidence plane is shown in Fig. 6. It can be noted that the crude PO approximation (dashed line) fails in predicting even the amplitude of the first side lobe.

In the previous case the dominating guided mode was a bound SW. This mode does not radiate directly, but affects the far-field pattern by virtue of the diffraction at the truncation of the array. A change in the nature of the guided wave may happen when the frequency is varied. When one of the spatial harmonics associated to the guided wave enters the visible region, the wave becomes a radiating LW, with a complex propagation constant. To describe this phenomenon and its effects on the array performance, we refer to a 19×19 array of dipoles, with length $L = 0.39$ cm, width $W = 0.01$ cm, and periodicity $d_x = d_y = 0.6$ cm, printed on a dielectric substrate with thickness $h = 0.1$ cm and relative permittivity $\varepsilon_r = 2.55$. The array is illuminated by an incident plane wave from broadside, at frequency $f = 30$ GHz. The diffracted and guided waves excited at the array edges propagate orthogonally to the edges. The dominant TM guided wave is excited at the y-oriented edges of the array (direction of propagation along the dipoles), while it is not excited at the x-oriented edges, due to the polarization mismatch (direction of propagation orthogonal to the dipoles). The solution of the dispersion equation with $k_y^{GW} = 0$, yields the propagation constant of the dominant TM mode of the structure.

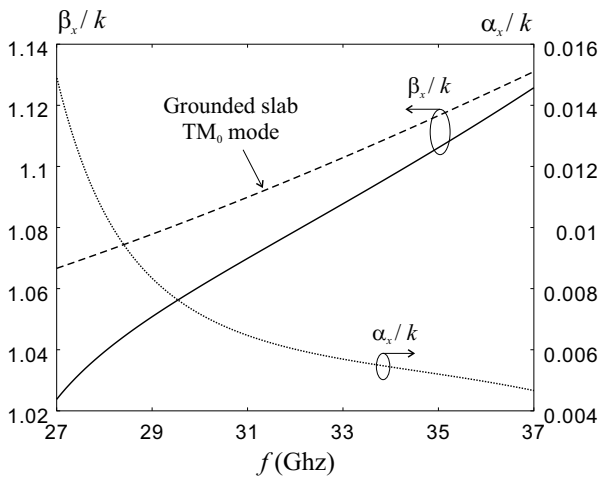

Fig. 7. Normalized phase (solid line) and attenuation (dotted line) constants of the fundamental harmonic $(p, q) = (0, 0)$ of the dominant TM mode versus frequency for the infinite periodic array of printed dipoles, with $L = 0.39$ cm, $W = 0.01$ cm, $d_x = 0.6$ cm, $d_y = 0.6$ cm, $\varepsilon_r = 2.55$, and $h = 0.1$ cm. Propagation along x direction is considered. Also the normalized propagation constant of the dominant TM_0 mode of the grounded dielectric slab is plotted (dashed line).

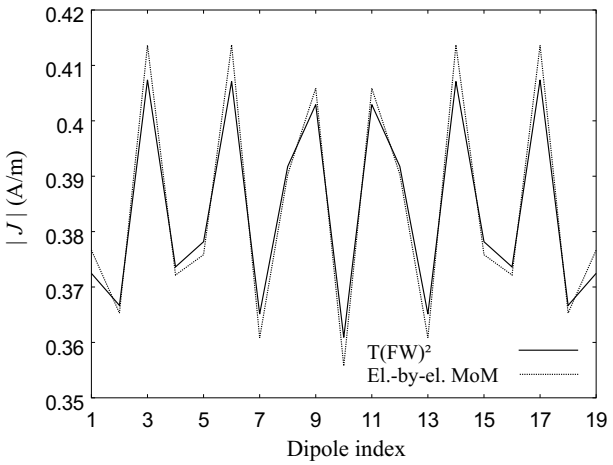

Fig. 8. Magnitude (in A/m) of the surface electric current sampled at the centers of the dipoles on the central row of the array. Results refers to a 19×19 array of dipoles, with $L = 0.39$ cm, $W = 0.01$ cm, $d_x = d_y = 0.6$ cm, $h = 0.1$ cm and $\varepsilon_r = 2.55$. The array is excited by a broadside incident plane wave at frequency $f = 30$ GHz.

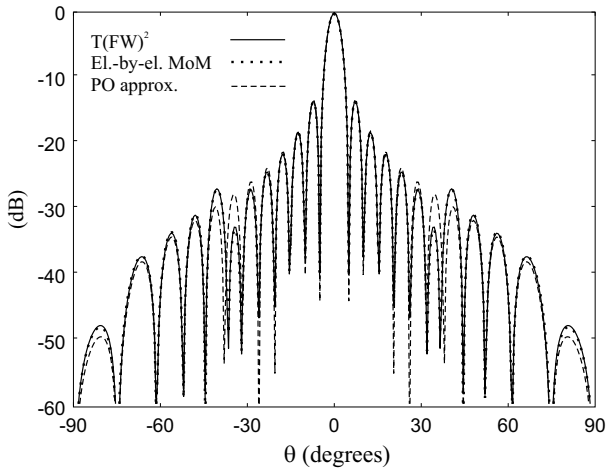

Fig. 9. Normalized magnitude of the θ-component of the electric field scattered by the array on the E-plane, for broadside plane-wave incidence. Results refers to the 19×19 array of dipoles of Fig. 8.

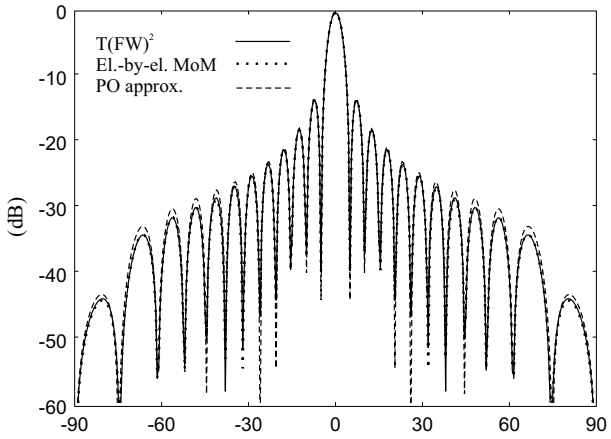

Fig. 10. Normalized magnitude of the ϕ-component of the electric field scattered by the array on the H-plane, for broadside plane-wave incidence. Results refers to the 19×19 array of dipoles of Fig. 8.

The $\beta - f$ diagram in Fig. 7, shows the behavior of the normalized phase and attenuation constants of the fundamental harmonic $(p, q) = (0, 0)$ of the wave in the frequency range $(27 - 37)$ GHz, together with the behavior of the normalized phase constant of the TM_0 surface wave of the grounded bare dielectric slab. At the operating frequency, the value of the propagation constant of the fundamental harmonic is $\beta_{x,00} - j\alpha_x = (1.0607 - j0.0071)k$. The $(p, q) = (-1, 0)$ spatial harmonic of the dominant TM mode is in the $\beta_x < 0$ zone of the fast-wave

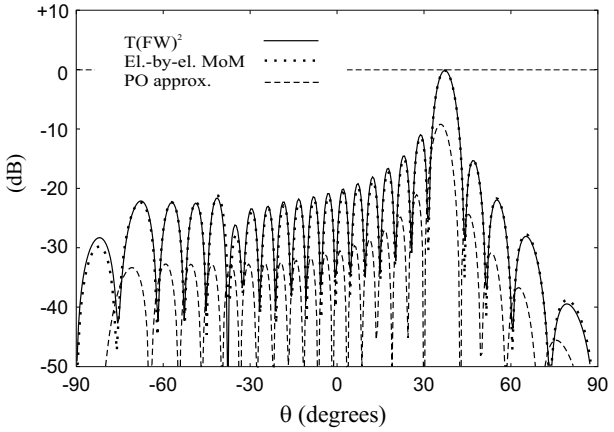

Fig. 11. Normalized magnitude of the θ-component of the electric field scattered by the array on the E-plane, for ($\varphi = 0^o$, $\theta_0 = 36^o$) plane-wave incidence. Results refers to the 19×19 array of dipoles of Fig. 8.

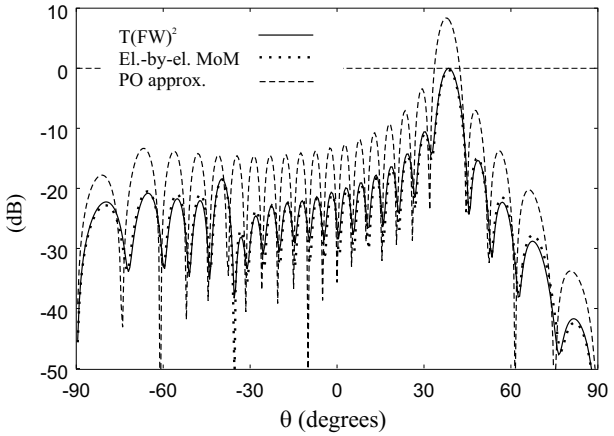

Fig. 12. Normalized magnitude of the θ-component of the electric field scattered by the array on the E-plane, for ($\varphi = 0^o$, $\theta_0 = 38^o$) plane-wave incidence. Results refers to the 19×19 array of dipoles of Fig. 8.

region; thus, representing a backward radiating LW, with the imaginary part of the propagation constant associated to the leakage of power. The direction of maximum radiation of the LW, computed through the relationship $\theta_{LW} \approx \sin^{-1}(\beta^{LW}_{x,-1,0}/k)$, is ± 37.6 degrees.

The results obtained with the present technique (solid line) are compared with the reference element-by-element MoM solution (dotted line). Fig. 8 presents the amplitude of the electric current at the center of the dipoles along the central row of the array. Fig. 9 shows the normalized scattered far field on the E-plane. The dip, noticeable in the far-field pattern around ± 37.6 degrees, is due to the interference between the PO field and the field radiated by the $(p, q) = (-1, 0)$ harmonic of the dominant LW mode excited at the two edges of the array (those orthogonal to the dipoles). In the case of a phased array antenna, this kind of LW is responsible for the scan-blindness phenomenon. Clearly, this effect cannot be predicted by a crude PO approximation (dashed line in Fig. 9), since it neglects the excitation of guided waves. Leaky wave radiation is absent on the H-plane, as shown in the far-field pattern of Fig. 10, due to the fact that the leaky-wave pattern has a null on this plane (analogously to the case of a TM mode excited by a dipole on a grounded dielectric slab). In order to better appreciate the effects of the LW radiation on the scattered field, two additional cases are considered with a plane wave incident along the E-plane ($\varphi = 0^o$) from directions $\theta_0 = 36$ and $\theta_0 = 38$ degrees, that are slightly below and above the LW radiation direction. Far-field results are shown in Fig. 11 and Fig. 12, and are normalized with respect to the maximum of the actual scattered field. In both cases, it is evident how the PO approximation dramatically fails in predicting the correct field. In particular, for incidence at $\theta_0 = 36$ degrees, the PO scattered field maximum is about 9 dB below the actual field maximum. Moreover, the direction of the maximum is shifted of about 1.5 degrees. On the contrary, for incidence at $\theta_0 = 38$ degrees, the PO scattered field maximum is about 8 dB above the actual field maximum, with a shift of 0.5 degrees. These results demonstrate how the infinite array approximation can lead to erroneous results in certain conditions.

VI. CONCLUSIONS

This paper presented a study on the edge effects in large periodic microstrip arrays. The analysis is performed through a hybrid numerical-asymptotic method, which allows to efficiently compute the fringe current excited at the truncation of the array. Based on physical considerations, this fringe current is expanded in terms of array-domain diffracted and guided wave basis functions. The unknown coefficients are found through the numerical solution

of a linear system, where the number of unknowns is completely independent of the number of elements in the array. Thus, this method constitutes an efficient and effective technique to analyze large arrays. Moreover, it provides a deep physical insight into the truncation effects of large periodic microstrip arrays, which can be an aid during the design stage of a practical array. The technique has been applied to the simple case of an array of microstrip dipoles, in order to highlight the fundamental effects. The generalization to more general shapes of the radiating element and to arbitrary stratified dielectric layers can be performed following the criteria furnished in this paper.

REFERENCES

[1] D. M. Pozar and D. H. Shaubert, "Scan blindness in infinite phased arrays of printed dipoles," *IEEE Trans. Antennas Propagat.*, vol. AP-32, no. 6, pp. 602-610, Jun. 1984.

[2] J.-M. Jin and J. L. Volakis, "Electromagnetic scattering by a perfectly conducting patch array on a dielectric slab," *IEEE Trans. Antennas Propagat.*, vol. 38, no. 4, pp. 556-563, Apr. 1990.

[3] G. H. Knittel, A. Hessel, and A. A. Oliner, "Element pattern nulls in phased arrays and their relation to guided waves," *IEEE Proceedings*, vol. 56, no. 11, pp. 1822-1836, Nov. 1968.

[4] D. S. Janning and B. A. Munk, "Effects of surface waves on the currents of truncated periodic arrays," *IEEE Trans. Antennas Propagat.*, vol. 50, no. 9, pp. 1254-1265, Sep. 2002.

[5] P. Pirinoli, L. Matekovits, G. Vecchi, F. Vapiana, and M. Orefice, "Synthetic functions: multiscale MoM analysis of arrays," *Proceedings of the 2003 IEEE Antennas Propagat. Society Symposium*, vol. 4, pp. 799-802, Columbus, 22-27 June 2003.

[6] J. Yeo and R. Mittra, "Numerically efficient analysis of microstrip antennas using the characteristic basis function method (CBFM)," *Proceedings of the 2003 IEEE Antennas Propagat. Society Symposium*, vol. 4, pp. 85-88, Columbus, 22-27 June 2003.

[7] A. Neto, S. Maci, G. Vecchi, and M. Sabbadini, "A truncated Floquet wave diffraction method for the full-wave analysis of large phased arrays, Part I: Basic principles and 2D case," *IEEE Trans. Antennas Propagat.*, vol. 48, no. 4, pp. 594-600, Apr. 2000.

[8] A. Neto, S. Maci, G. Vecchi, and M. Sabbadini, "A truncated Floquet wave diffraction method for the full-wave analysis of large phased arrays, Part II: generalization to the 3D case," *IEEE Trans. Antennas Propagat.*, vol. 48, no. 4, pp. 601-610, Apr. 2000.

[9] A. Cucini, M. Albani, and S. Maci, "Truncated Floquet wave full-wave ($\mathrm{T(FW)^2}$) analysis of large periodic arrays of rectangular waveguides," *IEEE Trans. Antennas Propagat.*, vol. 51, no. 6, pp. 1373-1385, Jun. 2003.

[10] A. Cucini, M. Albani, and S. Maci, "Truncated Floquet wave full-wave analysis of large phased arrays of open-ended waveguides with non-uniform amplitude excitation," *IEEE Trans. Antennas Propagat.*, vol. 51, no. 6, pp. 1386-1394, Jun. 2003.

[11] F. Capolino, M. Albani, S. Maci, and L. B. Felsen, "Frequency domain Green's function for a planar periodic semi-infinite phased array. Part I: Truncated Floquet wave formulation," *IEEE Trans. Antennas Propagat.*, vol. 48, no. 1, pp. 67-74, Jan. 2000.

[12] F. Capolino, M. Albani, S. Maci, and L. B. Felsen, "Frequency domain Green's function for a planar periodic semi-infinite phased array. Part II: Diffracted wave phenomenology," *IEEE Trans. Antennas Propagat.*, vol. 48, no. 1, pp. 75-85, Jan. 2000.

[13] F. Capolino, S. Maci, and L. B. Felsen, "Asymptotic high-frequency Green's function for a planar phased sectoral array of dipoles," *Wave Motion,*, vol. 34, no. 3, pp. 263-279, Sep. 2001.

[14] A. Polemi, A. Toccafondi, and S. Maci, "High-frequency Green's function for a semi-infinite array of electric dipoles on a grounded slab. Part I: Formulation," *IEEE Trans. Antennas Propagat.*, vol. 50, no. 12, pp. 1667-1677, Dec. 2001.

[15] H.-Y. D. Yang, K. Reonghee, and D. R. Jackson, "Design considerations for modeless integrated circuit substrates using planar periodic patches," *IEEE Trans. Microwave Theory Tech.*, vol. 48, no. 12, pp. 2233-2239, Dec. 2000.

[16] P. Lampariello, F. Frezza, and A. A. Oliner, "The transition region between bound-wave and leaky-wave ranges for a partially dielectric-

loaded open guiding structure," *IEEE Trans. Microwave Theory Tech.*, vol. 38, no. 12, pp. 1831-1836, Dec. 1990.

[17] J. L. Blanchard, E. H. Newman, M. E. Peters, "Integral equation analysis of artificial media," *IEEE Trans. Antennas Propagat.*, vol. 42, no. 5, pp. 727-731, May 1994.

[18] A. Cucini, S. Maci, and G. Vecchi, "Macro-scale modulation of local synthetic functions for large finite arrays and FSS," *28th ESA Antenna Workshop on Space Antenna Systems and Technologies*, Noordwijk, The Netherlands, 31 May - 3 June, 2005.

Alessio Cucini was born in Poggibonsi, Italy, in 1973. He received the Laurea degree (cum laude) in telecommunications engineering and the Ph.D. degree in electromagnetic engineering from the University of Siena, Italy, in 1999 and 2003, respectively. He is currently a Research Associate at the Department of Information Engineering, University of Siena, Italy. He is also with WaveComm S.r.l., a company operating in the field of electromagnetic software, antennas, sensors, and RF and microwave systems.

His research interests are in the area of applied electromagnetics, focused on numerical and asymptotic methods for phased arrays, frequency selective surfaces, EBG structures, artificial surfaces and microstrip antennas. Since 1999, he has been involved in projects of the European Space Agency (ESA) and of the European Community regarding software for antenna simulation.

Stefano Maci was born in Rome, Italy, in 1961. He received the laurea degree (cum laude) in electronic engineering from the University of Florence, Italy, in 1987. From 1990 to 1998, he was with the Department of Electronic Engineering, University of Florence, as an Assistant Professor. Since 1998, he has been an Associate Professor at the University of Siena, Italy. In 2004 he won the national competition for Full Professor.

His research interests include electromagnetic engineering, mainly concerned with high-frequency and numerical methods for antennas and scattering problems. He was a co-author of an incremental theory of diffraction, for the description of a wide class of electromagnetic scattering phenomena at high frequency, and of a diffraction theory for the high-frequency and hybrid analysis of large truncated periodic structures.

He has been and presently is responsible for several research contracts and projects supported by the European Union, by the European Space Agency (ESA-ESTEC, Noordvjiik, The Netherlands), and by various industry and research centers. In the sixth EU framework program, he is responsible of the European School of Antennas in the Antenna Center of Excellence. He was an Associate Editor of IEEE TRANSACTIONS ON ELECTROMAGNETIC COMPATIBILITY. He is presently a member of the Technical Advisory Board of the URSI Commission B and a member of the advisory board of the Italian Ph.D. School of Electromagnetism. He organized and/or served as a chairman for several special sessions at international conferences and has been chairman of two international workshops. Dr. Maci is principal author or co-author of about 45 papers in IEEE Journals, 50 papers in other international journals, and more than 200 papers in proceedings of international conferences.